ChemPubSoc Europe

DOI: 10.1002/chem.201903915

CHEMISTRY A European Journal Full Paper

Silver-Mediated Base Pairs

Silver-Mediated Homochiral and Heterochiral α-dC/β-dC Base Pairs: Synthesis of α-dC through Glycosylation and Impact of Consecutive, Isolated, and Multiple Metal Ion Pairs on DNA Stability

Yingying Chai[+,[a, c]] Peter Leonard[+,[a]] Xiurong Guo[+,[a]] and Frank Seela*[a, b]

Abstract: Isolated and consecutive heterochiral α-dC– base pairs have been incorporated into 12-mer oligonucleotide duplexes at various positions, thereby replacing Watson–Crick pairs. To this end, a new synthesis of the α-D anomer of dC has been developed, and oligonucleotides containing α-dC residues have been synthesized. Silver-mediated base pairs were formed upon the addition of silver ions. Furthermore, we have established that heterochiral α-dC–dC base pairs can approach the stability of a Watson–Crick pair, whereas homochiral dC–dC pairs are significantly less stable. A positional change of the silver-mediated base pairs affects the duplex stability and reveals the nearest-neighbor influence. When the number of silver ions was equivalent to the number of duplex base pairs (12), non-melting silver-rich complexes were formed. Structural changes have been supported by circular dichroism (CD) spectra, which showed that the B-DNA structure was maintained whilst the silver ion concentration was low. At high silver ion concentration, silver-rich complexes displaying different CD spectra were formed.

Introduction

Silver-mediated base pairs are attractive for the detection of DNA, for diagnostic purposes, and the construction of nanodevices.[1] Silver-ion DNA-binding motifs were first suggested more than 50 years ago, including those with silver ions positioned within base pairs.[2] In 2004, Ono discovered that the dC–dC mismatch selectively binds silver ions and forms stable silver-mediated base pairs.[3] Later, a single-crystal X-ray analysis was reported by the same author, which showed that the silver ions bridge the two N-3 atoms of the dC–dC mismatch.[4] Extremely stable pyrrolo–dC and imidazolo–dC pairs have been constructed in our laboratory, which demonstrated that the melting temperature (T_m) of a 12-mer duplex could be increased by more than 30 °C by the single incorporation of a silver-mediated base pair.[5] In 2017, an X-ray structure in which canonical base pairs were replaced by silver-ion-mediated base pairs was published.[6] This modification resulted in the formation of a duplex with silver ions positioned in the core of the DNA double helix, and aggregation of the duplex to a wire. Furthermore, the formation of silver-mediated c^7G_d–dC and c^7A_d–dT pairs (c^7G_d = 7-deaza-2′-deoxyguanosine, c^7A_d = 7-deaza-2′-deoxyadenosine) has been reported,[7] and many other artificial bases forming silver-mediated base pairs have also been studied.[1h,8]

Recently, our research group has shown that the anomeric heterochiral α-dC/β-dC pair is more stable than the homochiral β-dC/β-dC and α-dC/α-dC pairs.[9] In a later study, the influence of bulky cytosine substituents, such as in α-D-5-iodo-2′-deoxycytidine and α-D-5-octadiynyl–dC, was investigated.[10] Stability changes were observed when the position of the metal-mediated pair in the DNA molecule was altered. In these studies, only one silver-mediated α-dC/β-dC pair was incorporated in DNA, replacing a canonical Watson–Crick pair. In the present work, the impact of consecutive, isolated, and multiple incorporations of heterochiral α-dC/β-dC silver ion pairs on the stability of 12-mer duplexes is examined. The results are compared to those obtained for their homochiral β-dC/β-dC and α-dC/α-dC counterparts (Figure 1). Furthermore, the amount of

[a] Y. Chai,[+] P. Leonard,[+] X. Guo,[+] Prof. Dr. F. Seela
Laboratory of Bioorganic Chemistry and Chemical Biology
Center for Nanotechnology, Heisenbergstrasse 11
48149 Münster (Germany)
E-mail: Frank.Seela@uni-osnabrueck.de
Homepage: http://www.seela.net

[b] Prof. Dr. F. Seela
Laboratorium für Organische und Bioorganische Chemie
Institut für Chemie neuer Materialien, Universität Osnabrück
Barbarastrasse 7, 49069 Osnabrück (Germany)

[c] Y. Chai[+]
Department of Respiratory and Critical Care Medicine
Targeted Tracer Research and Development Laboratory
West China Hospital, Sichuan University, Sichuan, 610041 (P. R. China)

[+] These authors contributed equally to this work.

Supporting information and the ORCID identification number for the author of this article can be found under: https://doi.org/10.1002/chem.201903915.

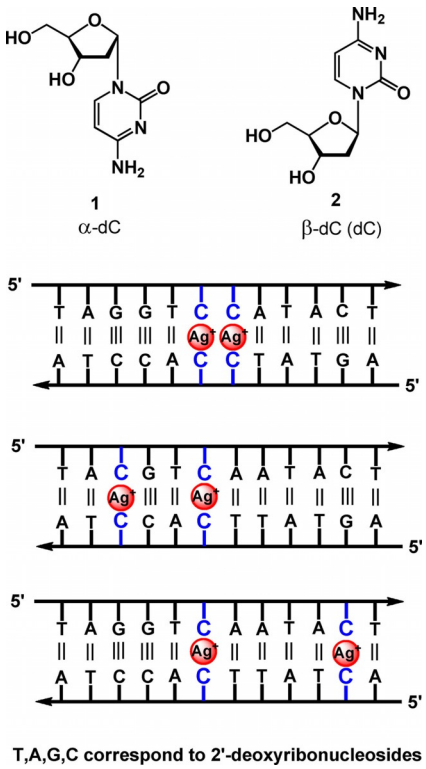

Figure 1. Top: α/β-D anomeric dC nucleosides used in this study. Bottom: Schematic representation of duplexes incorporating silver-mediated heterochiral α/β-dC base pairs.

bound silver ions per base pair has been determined by spectrophotometric titrations. An increase in the amount of silver ions beyond that corresponding to the mismatch binding sites gave further information on the process of silver-ion binding to 12-mer duplexes.

As our studies required sufficient amounts of α-dC (**1**), an efficient synthesis of **1** was developed, in which the α anomer is formed at the glycosylation stage. The predominant formation of the α anomer was initiated by aging Hoffer's α-D halogenose[11] to an anomeric mixture, which formed the α-anomeric nucleoside in excess. This new protocol, which is related to earlier work,[12] avoids the use of mercury salts to promote the glycosylation reaction. Finally, the α-dC was converted into a phosphoramidite, which was employed in solid-phase oligonucleotide synthesis.

Synthesis of α-dC by glycosylation

The existing routes for the synthesis of **1** involve 1) the conversion of ribo or arabino nucleosides to **1** via anhydro nucleosides as intermediates followed by 2′-deoxygenation;[13] 2) anomerization of protected β-dC (**2**) under acidic conditions,[14] 3) direct glycosylation of a protected nucleobase with an activated deoxyribose moiety in the presence of a mercury salt,[12] and 4) glycosylation of pyrimidinones followed by conversion of α-dU to α-dC.[15]

These methods are associated with various drawbacks, such as multistep synthesis (routes i and iv), low overall yields (route ii), or laborious separation of the reaction mixture and the use of a toxic mercury salt as catalyst (route iii). More recently, a high-yielding synthesis of α-5-iodo-dC has been reported,[10] involving glycosylation of silylated 5-iodocytosine with a preaged sugar halide (Hoffer's halogenose)[11] according to conditions reported by Aoyama[16] for dU derivatives and by Walker[17] for the anomerization of deoxy sugars. In this case, final separation of the anomers was accomplished by conversion to their 5′-DMT (DMT = 4,4′-dimethoxytrityl) derivatives.[10]

In view of the promising results obtained with the iodo compound, we applied this route for the synthesis of **1**. First, cytosine was silylated with 1,1,1,3,3,3-hexamethyldisilazane (HMDS)/trimethylsilyl chloride (TMSiCl) and then the silylated base was glycosylated with the Hoffer halogenose **4** in CH_2Cl_2 using pyridine and *p*-nitrophenol as catalysts (for details, see the Experimental Section). After purification of the reaction mixture by flash column chromatography, an inseparable mixture of anomers **5** and **6** was obtained in 84% yield. A 2:1 α/β ratio was determined by ^{1}H NMR spectroscopy, comparing the intensities of the H-1′ signals. The mixture was deprotected (0.2 M NaOMe/MeOH) to afford an anomeric mixture of α/β-dC, which proved to be inseparable by column chromatography (94% yield for deprotection, 79% overall yield based on **3**). The synthesis was also performed in one step without isolation of the toluoylated intermediates, giving α/β-dC in 81% overall yield. Attempts to separate the anomers after 4,4′-dimethoxytritylation were cumbersome. In another approach, the amino groups of α/β-dC were protected with benzoyl residues. The anomers could then be separated, furnishing benzoylated (Bz)-α-dC (**7**) in 36% yield and Bz-β-dC (**8**) in 22% yield. Compound **7** was then converted into the DMT derivative **9**[18] (90% yield). Phosphitylation of **9** gave **10** in 81% yield. The free nucleoside **1** was obtained in 81% yield by deprotection of **7** in saturated NH_3/MeOH at 100 °C (Scheme 1). Following this route, **1** could be synthesized in multigram amounts in three steps from **4** in an overall yield of 24%. The reported synthesis represents a valuable method for the large-scale preparation of α-dC, whereby it is obtained convergently from the protected base and the halogenose **4**.

All of the synthesized compounds were characterized by their ^{1}H and ^{13}C NMR spectra and their ESI-TOF mass spectra (see the Experimental Section). ^{1}H–^{13}C correlated (HMBC and HSQC) NMR spectra were used to assign the ^{13}C NMR signals. For details, see the Supporting Information (Table S1, Figures S18–S54). NOESY measurements (Figures S48 and S54, Supporting Information) showed an NOE of the H_β-2′ signal upon irradiation of H-1′, providing evidence for the α-D configuration of **1**, whereas an NOE of the H_α-2′ signal was observed for **2**. Furthermore, differences in chemical shifts were observed in the ^{1}H and ^{13}C NMR spectra of α-dC and β-dC. The signals of H_β-2′, H-4′, and H-5 of α-D anomers are shifted downfield ($\Delta\delta = 0.4$–0.5 ppm) compared to those of the β-D compounds, whereas the signals of H-1′, H-5′, H_α-2′, and H-6 are shifted upfield ($\Delta\delta = 0.1$–0.2 ppm). In the ^{13}C NMR spectrum of α-dC, the C-1′ and C-4′ signals are shifted upfield ($\Delta\delta = 1.6$ and 1.9 ppm).

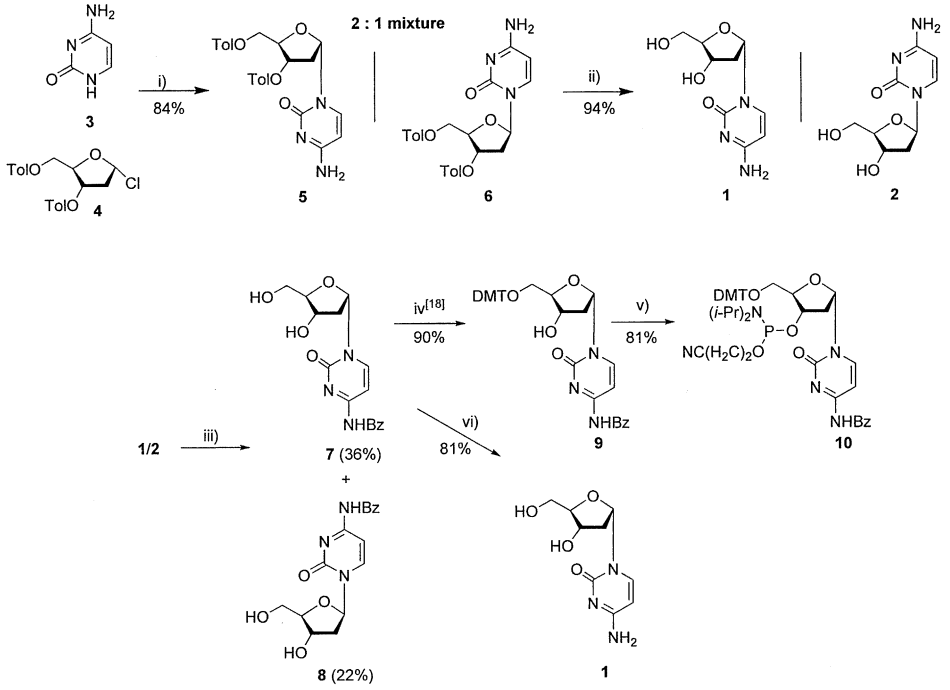

Scheme 1. Synthesis of α-dC (**1**): i) a) HMDS, TMSiCl, reflux, 2 h; b) addition of Hoffer's sugar **4**,[11] pyridine, *p*-nitrophenol, CH_2Cl_2, RT, 24 h; ii) NaOMe, MeOH, RT, 1 h; iii) $(Bz)_2O$, DMF, RT, 48 h; iv) DMT-Cl, pyridine, RT, 3 h; v) 2-cyanoethyl *N*,*N*′-diisopropylphosphoramidochloridite, DIPEA, CH_2Cl_2, RT, 30 min; vi) NH_3/MeOH, 100 °C, 16 h.

Oligonucleotide syntheses and characterization

Oligonucleotides (ODNs) containing α-D-2′-deoxycytidine (**1**) were prepared by solid-phase synthesis employing the phosphoramidite **10** together with standard building blocks.

The 2′-deoxycytidine α and β anomers **1** and **2** were incorporated at different positions of the 12-mer duplex 5′-d(TAGGTCAATACT) (ODN-**1**)·3′-d(ATCCAGTTATGA) (ODN-**2**), replacing canonical base pairs. ODN-**1**·ODN-**2** represents a standard duplex, and has been used in our laboratory to study silver-mediated base pairing with a number of nucleoside analogues. After solid-phase synthesis, the oligodeoxyribonucleotides were cleaved from the solid support, and then deprotected in concentrated (28%) aqueous ammonia (55 °C for 2 h) and at RT overnight. The coupling yields of the modified building blocks were consistently higher than 95%. All synthesized

Table 1. Synthesized oligonucleotides and their molecular masses determined by MALDI-TOF mass spectrometry.

Entry	Oligonucleotides	M_r calcd[a] M_r found[b]	Entry	Oligonucleotides	M_r calcd[a] M_r found[b]
ODN-**1**	5′-d(TAGGT**CA**ATACT)[8d]	3643.6 3643.7	ODN-**10**	5′-d(TAGGT$^{\alpha}$**C**AATA$^{\alpha}$**C**T)	3645.4 3645.1
ODN-**2**	5′-d(AGTAT**TG**ACCTA)[8d]	3643.6 3643.7	ODN-**11**	5′-d(TAGGT$^{\alpha}$**C**$^{\alpha}$**C**ATACT)	3621.4 3621.2
ODN-**3**	5′-d(TAGGT**CC**ATACT)	3621.4 3621.3	ODN-**12**	5′-d(TACGTCAATACT)	3605.4 3606.6
ODN-**4**	5′-d(AGTAT**CC**ACCTA)	3590.4 3590.5	ODN-**13**	5′-d(AGTAT$^{\alpha}$**C**$^{\alpha}$**C**ACCTA)	3590.4 3589.9
ODN-**5**	5′-d(AGTATT**C**AC**C**TA)	3605.4 3603.9	ODN-**14**	5′-d(TAGGT$^{\alpha}$**C**AATACT)	3645.4 3644.7
ODN-**6**	5′-d(AGTATT$^{\alpha}$**C**AC$^{\alpha}$**C**TA)	3605.4 3604.7	ODN-**15**	5′-d(T^{7}**A**^{7}**G**^{7}**G**TC^{7}**A**^{7}**A**T^{7}**A**CT)[8d]	3638.7 3639.1
ODN-**7**	5′-d(TA$^{\alpha}$**C**GT$^{\alpha}$**C**AATACT)	3605.4 3603.5	ODN-**16**	5′-d(^{7}**A**^{7}**G**T^{7}**A**TT^{7}**G**^{7}**A**CCT^{7}**A**)[8d]	3638.7 3638.5
ODN-**8**	5′-d(A**C**TATT**C**ACCTA)	3565.4 3564.7	ODN-**17**	5′-d(GGA**C**TCGA**C**TCC)	3607.4 3606.8
ODN-**9**	5′-d(A$^{\alpha}$**C**TATT$^{\alpha}$**C**ACCTA)	3565.4 3564.9			

[a] Calculated on the basis of the molecular mass of $[M+H]^+$. [b] Determined by MALDI-TOF mass spectrometry as $[M+H]^+$ in linear positive mode. $^{\alpha}$C denotes α-D-2′-deoxycytidine (**1**). ^{7}A denotes 7-deaza-2′-deoxyadenosine, and ^{7}G denotes 7-deaza-2′-deoxyguanosine.

oligodeoxyribonucleotides were purified by reversed-phase HPLC (RP-18), detritylated with 2.5% dichloroacetic acid in dichloromethane, and further purified by HPLC. The contents giving rise to single peaks were isolated in all cases (Figure S17, Supporting Information). Subsequently, molecular masses were determined by MALDI-TOF mass spectrometry. All oligonucleotides used in this study and their masses are shown in Table 1.

Positional impact of consecutive and isolated silver-mediated heterochiral and homochiral cytosine base pairs on duplex stability

Recently, our research group reported on silver-mediated heterochiral α-dC/β-dC base pairs that bind more strongly than their homochiral dC/dC counterparts.[9] A 12-mer duplex with single incorporation of a silver-mediated α-dC/β-dC pair showed significantly higher thermal stability ($T_m = 43\,^{\circ}C$) than that with a homochiral β-dC–Ag^+–β-dC pair ($T_m = 34\,^{\circ}C$). Furthermore, α-dC showed excellent mismatch discrimination in DNA single nucleotide polymorphism (SNP).[9] In this work, we investigate the impact of more than one heterochiral α-dC–Ag^+–β-dC base pair on the physical properties of the 12-mer duplex 5′-d(TAGGTCAATACT) (ODN-**1**)·3′-d(ATCCAGTTATGA) (ODN-**2**). For this, two dG–dC base pairs or one dG–dC and one dA–dT base pair were replaced by silver-mediated heterochiral α-dC/β-dC pairs. Oligonucleotide duplexes containing two sequential or two isolated α-dC–Ag^+–β-dC pairs were constructed (Table 2). Furthermore, the silver-mediated base pairs were shifted along the 12-mer duplex. For comparison, oligonucleotide duplexes with silver-mediated homochiral β-dC/β-dC or α-dC/α-dC were prepared, and the homochiral dC/dC pairs were incorporated at exactly the same positions as the heterochiral pairs. Silver-mediated base-pair formation with homochiral and heterochiral base pairs was studied, and T_m measurements were performed in 100 mM NaOAc/10 mM $Mg(OAc)_2$ at pH 7.4. Typical melting profiles are displayed in Figure 1. Heating and cooling curves are shown in the Supporting Information (Figures S1–S7). In the absence of silver ions, only the 12-mer duplexes containing heterochiral pairs showed almost complete melting profiles from which T_m values could be determined; from the profiles of the duplexes with homochiral dC/dC pairs, T_m values could only be determined in a few cases. When two silver ions were added to homochiral or heterochiral duplexes, almost all duplexes displayed melting curves from which T_m values could be deter-

Table 2. T_m values of oligonucleotide duplexes containing two consecutive or isolated α-dC/dC heterochiral or α-dC/α-dC or β-dC/β-dC homochiral base pairs in the presence and absence of silver ions.[a]

Duplexes **β/β-D and α/α-D homochiral base pairs consecutive**	T_m [°C]	T_m [°C] +2 Ag^+/duplex (ΔT_m [°C])	T_m [°C] +4 Ag^+/duplex (ΔT_m [°C])	Duplexes **α/β-D heterochiral base pairs consecutive**	T_m [°C]	T_m [°C] +2 Ag^+/duplex (ΔT_m [°C])	T_m [°C] +4 Ag^+/duplex (ΔT_m [°C])
5′-d-(TAGGT**CA**ATACT) (ODN-**1**) 3′-d-(ATCCA**GT**TA TGA) (ODN-**2**)	47.0	48.0 (+1.0)	47.0 (±0)	5′-d-(TAGGT**CA**ATACT) (ODN-**1**) 3′-d-(ATCCA**GT**TATGA) (ODN-**2**)	47.0	48.0 (+1)	47.0 (±0)
5′-d-(TAGGT**CC**ATACT) (ODN-**3** 3′-d-(ATCCA**CC**TATGA) (ODN-**4**)	no T_m	<20	<20	5′-d-(TAGGT**CC**ATACT) (ODN-**3**) 3′-d-(ATCCA$^{\alpha}$**C**$^{\alpha}$**C**TATGA) (ODN-**13**)	24.0	43.0 (+19.0)	43.0 (+19.0)
5′-d-(TAGGT$^{\alpha}$**C**$^{\alpha}$**C**ATACT) (ODN-**11**) 3′-d-(ATCCA$^{\alpha}$**C**$^{\alpha}$**C**TATGA) (ODN-**13**)	no T_m	<20	<20	5′-d-(TAGGT$^{\alpha}$**C**$^{\alpha}$**C**ATACT) (ODN-**11**) 3′-d-(ATCCA**CC**TATGA) (ODN-**4**)	26.0	43.0 (+17.0)	46.0 (+20.0)
β/β-D and α/α-D homo base pairs isolated				**α/β-D hybrid base pairs isolated**			
5′-d-(TAGGT**C**AATA**C**T) (ODN-**1**) 3′-d-(ATCCA**G**TTAT**G**A) (ODN-**2**)	47.0	48.0 (+1)	47.0 (±0)	5′-d-(TAGGT**C**AATA**C**T) (ODN-**1**) 3′-d-(ATCCA**G**TTAT**G**A) (ODN-**2**)	47.0	48.0 (+1)	47.0 (±0)
5′-d-(TAGGT**C**AATA**C**T) (ODN-**1**) 3′-d-(ATCCA**C**TTAT**C**A) (ODN-**8**)	<20	27.0 (+ >7.0)	27.0 (+ >7.0)	5′-d-(TAGGT**C**AATA**C**T) (ODN-**1**) 3′-d-(ATCCA$^{\alpha}$**C**TTAT$^{\alpha}$**C**A) (ODN-**9**)	21.5	38.0 (+16.5)	39.0 (+17.5)
5′-d-(TAGGT$^{\alpha}$**C**AATA$^{\alpha}$**C**T) (ODN-**10**) 3′-d-(ATCCA$^{\alpha}$**C**TTAT$^{\alpha}$**C**A) (ODN-**9**)	24.0	25.0 (+1.0)	25.0 (+1.0)	5′-d-(TAGGT$^{\alpha}$**C**AATA$^{\alpha}$**C**T) (ODN-**10**) 3′-d-(ATCCA**C**TTAT**C**A) (ODN-**8**)	24.0	40.0 (+16.0)	41.0 (+17.0)
5′-d-(TA**G**GT**C**AATACT) (ODN-**1**) 3′-d-(AT**C**CA**G**TTATGA) (ODN-**2**)	47.0	48.0 (+1)	47.0 (±0)	5′-d-(TA**G**GT**C**AATACT) (ODN-**1**) 3′-d-(AT**C**CA**G**TTATGA) (ODN-**2**)	47.0	48.0 (+1)	47.0 (±0)
5′-d-(TA**C**GT**C**AATACT) (ODN-**12**) 3′-d-(AT**C**CA**C**TTATGA) (ODN-**5**)	<20	26.5 (+ >6.5)	27.0 (+ >7.0)	5′-d-(TA**C**GT AATACT) (ODN-**12**) 3′-d-(AT$^{\alpha}$**C**CA$^{\alpha}$**C**TTATGA) (ODN-**6**)	23.0	40.0 (+17.0)	41.0 (+18.0)
5′-d-(TA$^{\alpha}$**C**GT$^{\alpha}$**C**AATACT) (ODN-**7**) 3′-d-(AT$^{\alpha}$**C**CA$^{\alpha}$**C**TTATGA) (ODN-**6**)	21.5	22.0 (+0.5)	25.0 (3.5)	5′-d-(TA$^{\alpha}$**C**GT$^{\alpha}$**C**AATACT) (ODN-**7**) 3′-d-(AT**C**CA**C**TTATGA) (ODN-**5**)	22.0	45.0 (+23.0)	46.0 (+24.0)

[a] Measured at 260 nm at a concentration of 5 μM + 5 μM single strand at a heating rate of 1.0 °C min^{-1} in 100 mM NaOAc/10 mM $Mg(OAc)_2$, pH 7.4, in the presence of various concentrations of $AgNO_3$ (0–4 silver ions/duplex). T_m values were calculated from the heating curves using the program Meltwin 3.0.[19] $\Delta T_m = T_m$ after the addition of $AgNO_3 - T_m$ before the addition of $AgNO_3$. $^{\alpha}$**C** denotes α-D-2′-deoxycytidine (**1**).

mined. Comparing the T_m curves shown in Figure 2, it is obvious that all duplexes incorporating two heterochiral α-dC/β-dC pairs (right column) were more stable than those containing homochiral dC/dC pairs (left column). When NaI was added to the silver ion/DNA solutions, the melting curves reverted to the original silver-free curves, indicating that the changes were not due to chemical modification.

Next, UV titration experiments were performed on both series (homochiral and heterochiral base pairs). From the curves depicted in Figure 3 and Figures S8 and S9 (Supporting Information), it is apparent that one silver ion is invariably bound to one heterochiral base pair.

Next, a set of duplexes with all possible homochiral α/α- and β/β-dC combinations, as well as with α/β-dC heterochiral

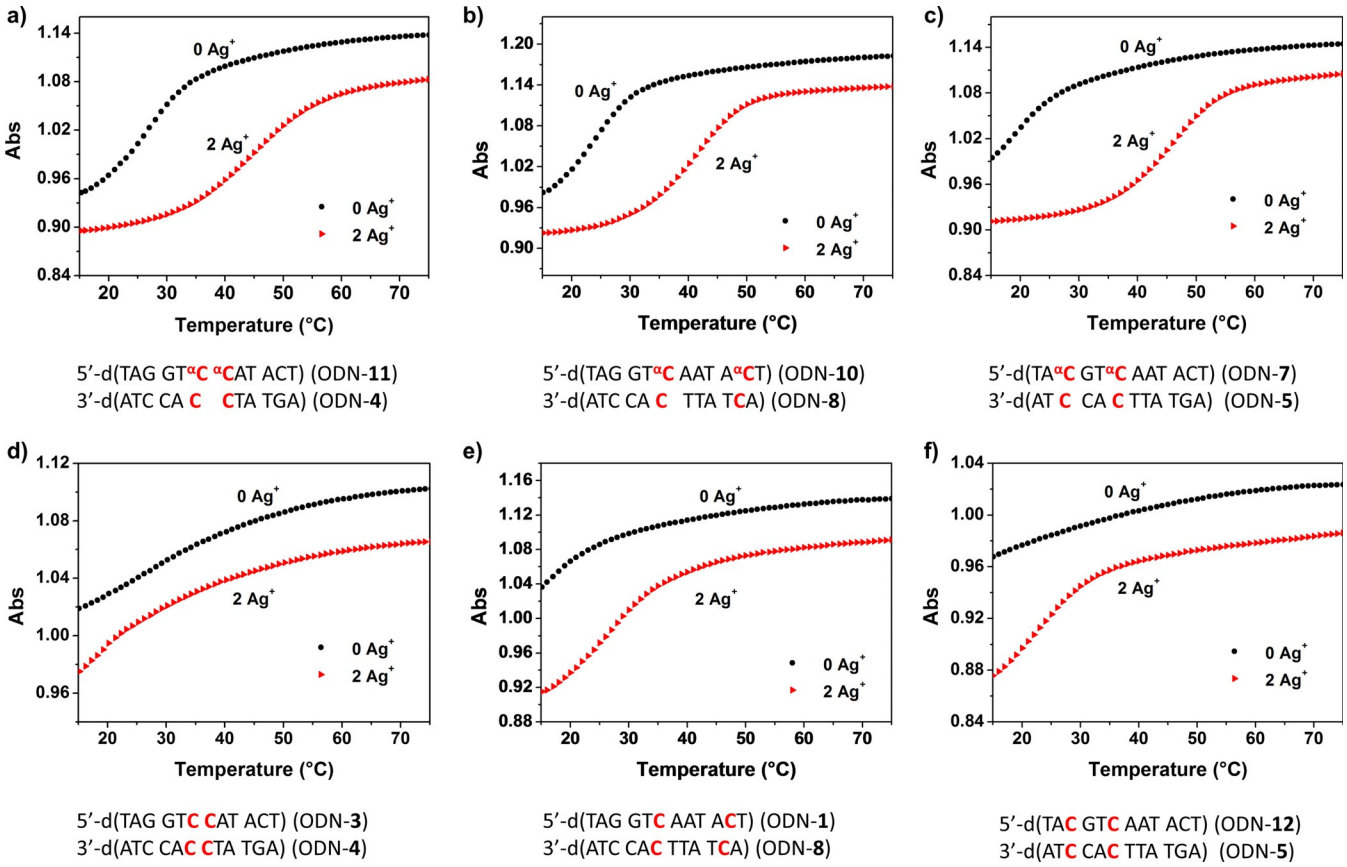

Figure 2. Thermal denaturation experiments were performed at a concentration of 5 μM + 5 μM single strand in buffer solution (100 mM NaOAc, 10 mM $Mg(OAc)_2$, pH 7.4), monitoring at 260 nm in the presence of various concentrations of Ag^+ (0 and 2 silver ions). Data were obtained from heating experiments: a) ODN-**11**·ODN-**4**; c) ODN-**10**·ODN-**8**; e) ODN-**7**·ODN-**5** containing α/β-dC heterochiral base pairs and b) ODN-**3**·ODN-**4**; d) ODN-**1**·ODN-**8**; f) ODN-**12**·ODN-**5** containing dC– homochiral base pairs.

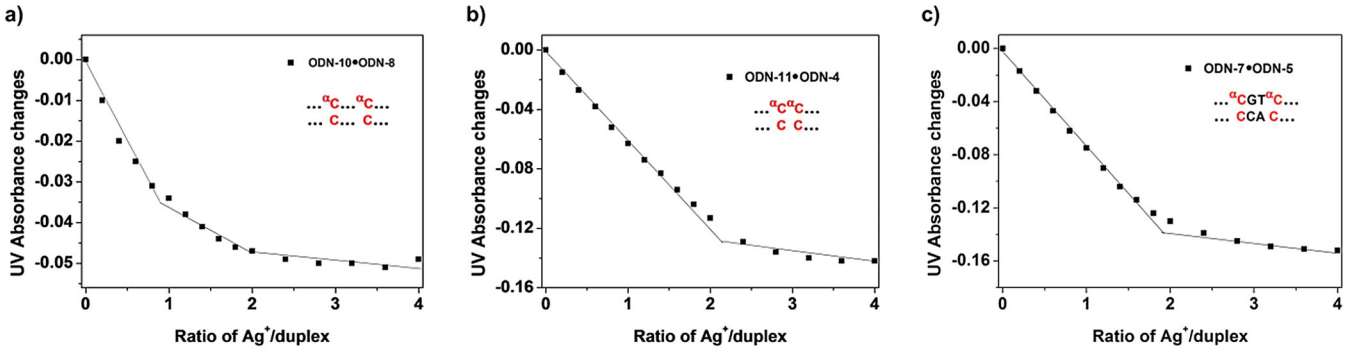

Figure 3. Titration graphs displaying changes in UV absorbance (measured at 260 nm) versus consumption of silver ions/duplex for the duplexes: a) ODN-**10**·ODN-**8**; b) ODN-**11**·ODN-**4**, and c) ODN-**7**·ODN-**5** containing α/β-dC heterochiral base pairs. All measurements were performed at a concentration of 5 μM + 5 μM single strand in 100 mM NaOAc, 10 mM $Mg(OAc)_2$, pH 7.4.

base pairs, was investigated (Table 2). The base-pair positions were changed between complementary strands. The positions were also shifted along the double-helix. The duplex stability was measured in the presence and absence of silver ions. From the data in Table 2, the following conclusions can be drawn.

1) The stability of a duplex formed exclusively by Watson–Crick base pairs is not changed by the presence of a small amount of silver ions (two). 2) All duplexes with silver-mediated heterochiral base pairs show melting profiles with T_m values significantly higher than those of their homochiral counterparts. 3) Duplexes with homochiral α/α-dC silver-mediated base-pair combinations are less stable than those with β/β-dC base pairs. (iv) A positional change of silver-mediated base pairs along the axis of the double-helix affects the T_m value of the duplex, indicating that nearest-neighbor effects play a role in heterochiral and homochiral silver-mediated base-pair formation.

Heterochiral base pairs

The highest T_m values were observed for duplexes containing heterochiral α/β-dC base pairs in consecutive positions (ODN-**11**·ODN-**4**) or separated by two canonical base pairs (ODN-**7**·ODN-**5**). In these cases, the duplex stability approaches that of the standard duplex. Here, α-dC is located in the upper strand and β-dC in the lower strand. Switching the positions of α-dC and β-dC leads to somewhat lower stability ($\Delta T_m = 3$–5 °C). The same is valid when one silver-mediated α/β-dC base pair is located near the middle of the duplex and the other is at a terminal position (ODN-**1**·ODN-**9**).

Homochiral base pairs

In the case of consecutive silver-mediated homochiral dC/dC base pairs, T_m values are low, irrespective of which combination of anomeric nucleosides is chosen (α/α or β/β, upper-left part of Table 2) and complete melting curves could not be obtained. Separated dC/dC silver-mediated pairs increased the T_m by 7.0 °C (ODN-**1**·ODN-**8**). In the case of separated α/α-dC pairs, a much smaller increase was observed (ODN-**6**·ODN-**7**). Mismatch combinations of α/α-dC pairs in the absence of silver ions are more stable ($T_m = 21$–24 °C) than the β/β combinations ($T_m < 20$ °C).

Previous work on homochiral dC–Ag^+–dC pairs may give the impression that the silver-mediated dC–dC pair is a strong base pair. This is indeed the case when the stability of the silver-mediated base pair is compared with that of the silver-free mismatch. However, the stability of a dC–Ag^+–dC pair falls short of those of Watson–Crick dA–dT or dG–dC pairs (Figure 4 top). On the contrary, silver-mediated heterochiral α/β-dC pairs approach the stability of Watson–Crick base pairs (Figure 4 bottom). The different behavior of silver-mediated homochiral and heterochiral base pairs with regard to Watson–Crick pairs is outlined in Figure 4.

It became evident that the stability of a duplex of identical length and composition decreases with increasing number of homochiral silver-mediated dC base pairs replacing canonical Watson–Crick pairs (Table 2, Figure 4 top). However, a much smaller decrease, or even no decrease, was observed for duplexes with heterochiral dC/dC silver-mediated base pairs. In this case, the silver-mediated cytosine base-pair stability is in the range of that of a Watson–Crick pair (Figure 5). For duplexes with one or two silver-mediated heterochiral dC/dC base pairs, the T_m values are almost identical (40–43 °C, Figure 5 a, b, Table S2, Supporting Information). However, this situation changes for homochiral silver-mediated dC/dC base pairs. Here, strong decreases are observed, with T_m values of 34 °C for the incorporation of one mismatch and 26 °C for two incorporations (Figure 5 c, Table S2, Supporting Information).

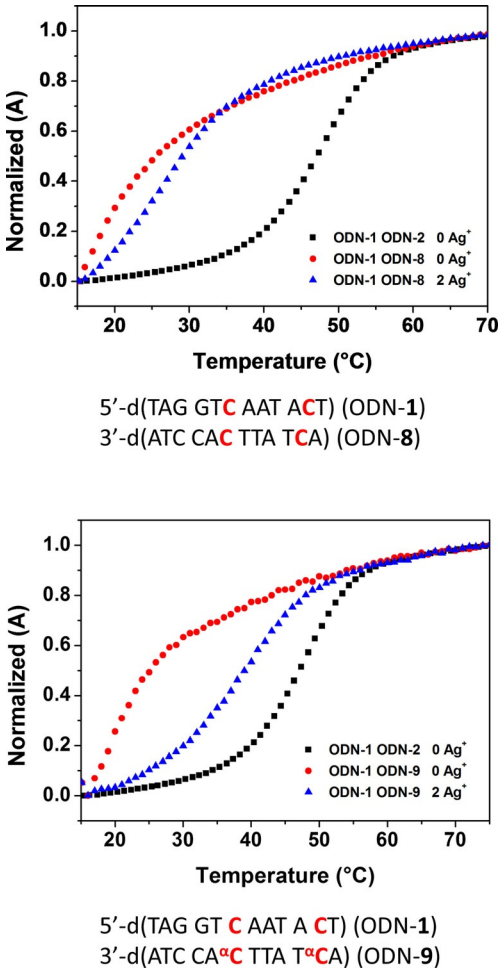

Figure 4. Thermal denaturation experiments performed at a concentration of 5 μM + 5 μM single strand in buffer solution (100 mM NaOAc, 10 mM $Mg(OAc)_2$, pH 7.4), monitoring at 260 nm in the presence of various concentrations of Ag^+ (0 and 2 silver ions): top) ODN-**1**·ODN-**8** containing dC–dC homochiral base pairs (red and blue lines) and bottom) ODN-**1**·ODN-**9** containing α/β-dC heterochiral base pairs (red and blue lines). The standard duplex ODN-**1**·ODN-**2** was used for comparison (black line).

Performance of duplexes upon increasing the amount of silver ions

Canonical DNA as well as low-molecular-weight oligonucleotide duplexes can adopt structures in which all Watson–Crick

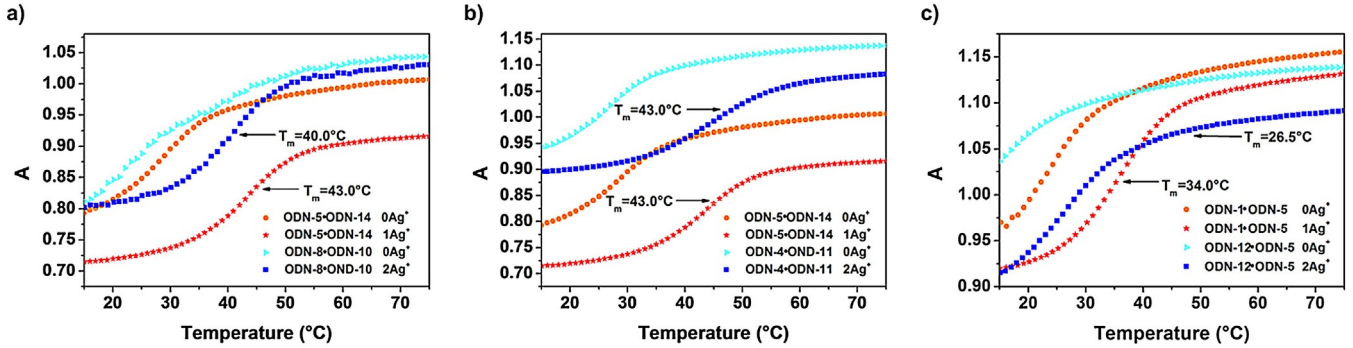

5'-d(TAG GT$^{\alpha}$C AAT ACT) (ODN-**14**) 5'-d(TAG GT$^{\alpha}$C AAT ACT) (ODN-**14**) 5'-d(TAG GTC AAT ACT) (ODN-**1**)
3'-d(ATC CAC TTA TGA) (ODN-**5**) 3'-d(ATC CA C TTA TGA) (ODN-**5**) 3'-d(ATC CAC TTA TGA) (ODN-**5**)

5'-d(TAG GT$^{\alpha}$CAAT A$^{\alpha}$CT) (ODN-**10**) 5'-d(TAG GT$^{\alpha}$C $^{\alpha}$CAT ACT) (ODN-**11**) 5'-d(TAC GTC AAT ACT) (ODN-**12**)
3'-d(ATC CA C TTA T CA) (ODN-**8**) 3'-d(ATC CA C CTA TGA) (ODN-**4**) 3'-d(ATC CAC TTA TGA) (ODN-**5**)

Figure 5. Thermal denaturation experiments performed at a concentration of 5 μM + 5 μM single strand in buffer solution (100 mM NaOAc, 10 mM $Mg(OAc)_2$, pH 7.4), monitoring at 260 nm in the presence of various concentrations of Ag^+ (0 and 2 silver ions per duplex): a) ODN-**14**•ODN-**5** and ODN-**10**•ODN-**8**; b) ODN-**14**•ODN-**5** and ODN-**11**•ODN-**4**; c) ODN-**1**•ODN-**5** and ODN-**12**•ODN-**5** containing dC–dC homochiral or α/β-dC heterochiral base pairs.

base pairs are converted into silver-mediated base pairs.[6a] Previous studies with high-molecular-weight DNA or enzymatically prepared polynucleotides indicated different binding sites, with N-7 of the guanine base as the preferred binding position. The formation of these structures depends on the amount of silver ions added. Previous reports also indicate that G–C-rich DNA binds silver ions more efficiently than G–C-poor DNA.[2f] Indeed, this phenomenon was applied to separate dG–dC-rich from dG–dC-poor DNA by ultracentrifugation.[2e]

The most efficient way of introducing silver ions in the core of a double-helix is the replacement of stable Watson–Crick pairs by labile nucleoside mismatches that selectively bind silver ions. Such mismatches are formed by homo base pairs of dT–dT, dC–dC, or dG–dG, as well as by the hetero pair of 5-aza-7-deaza-2′-deoxyguanosine with 2′-deoxycytidine.[20] A recent X-ray structure determination of a dodecamer duplex that could be expected to form silver-mediated dA–dT and dG–dC base pairs showed instead that silver-mediated homo pairs of dT–dT, dG–dG, and dC–dC were formed, and that the dA residues were looped out.[6a] Due to the different stabilities of bidentate dA–dT and tridentate dG–dC pairs, one may be preferentially converted into a silver-mediated pair. Nevertheless, as already discussed by Gwinn,[8g] silver-mediated homo pairs of dC–dC or dG–dG are more stable than silver-mediated dA–dT or dG–dC pairs. Accordingly, the process of silver-mediated base-pair formation is complex, can be sequence-dependent, and various structures can be formed in the presence of large amounts of silver ions. Other factors, such as argentophilic interactions, may also be of importance.

Based on these observations, we anticipated that our duplexes with two mismatches might also consume more silver ions, thereby forming silver-mediated base pairs between natural bases. Therefore, we set out to determine whether duplexes with homochiral or heterochiral dC mismatches can adopt other structures when the amount of silver ions is increased beyond the number of mismatches. For this, T_m measurements were performed, and the amount of silver ions was increased to one per base pair for a particular duplex. Duplex ODN-**10**•ODN-**8**, with two heterochiral α-dC/β-dC pairs and, for comparison, ODN-**1**•ODN-**8**, with two homochiral dC/dC pairs, were selected for this purpose. Homochiral and heterochiral silver-mediated pairs were located at exactly the same positions. Melting profiles and CD spectra were recorded after stepwise addition of silver ions. In initial experiments, duplexes without mismatches (ODN-**1**•ODN-**2**) or 7-deazapurine/pyrimidine base pairs (ODN-**15**•ODN-**16**) were investigated (Figure 6).

We have previously reported the structural changes induced by increasing numbers of silver ions in the 12-mer duplex ODN-**1**•ODN-**2** as well as in the duplex ODN-**15**•ODN-**16**, in which all purine bases are replaced by 7-deazapurine moieties.[8d] However, only a few data sets (addition of 6 and 12 silver ions) were given. As we wanted to compare these data with those for duplexes incorporating homochiral or heterochiral base pairs, silver ions were added in a stepwise manner (0–12 silver ions, Figure 6a, c). For a 12-mer duplex, 12 silver ions means that one silver ion is available for each base pair. Melting curves were then measured, heating and cooling cycles were recorded, and normalized melting curves were calculated. These data are documented in the Supporting Information (Figures S5–S7).

It was noticed that at higher silver ion concentrations the first temperature cycle showed hysteresis and sometimes two or three heating and cooling cycles had to be performed to obtain identical melting profiles (Figures S10–S13, Supporting Information). Only then was the system in equilibrium.

Figure 6a shows that an increased amount of silver ions caused an absorbance decrease of the otherwise sigmoidal melting profile of duplex ODN-**1**•ODN-**2**. Such a decrease occurs as the number of Watson–Crick base pairs decreases. Interestingly, the T_m of the duplex did not show a substantial change upon increasing the amount of silver ions (Figures S5–S7, Supporting Information); only the UV absorbance changed. Therefore, we conclude that upon addition of silver ions the number of Watson–Crick base-pair-rich duplexes decreases in

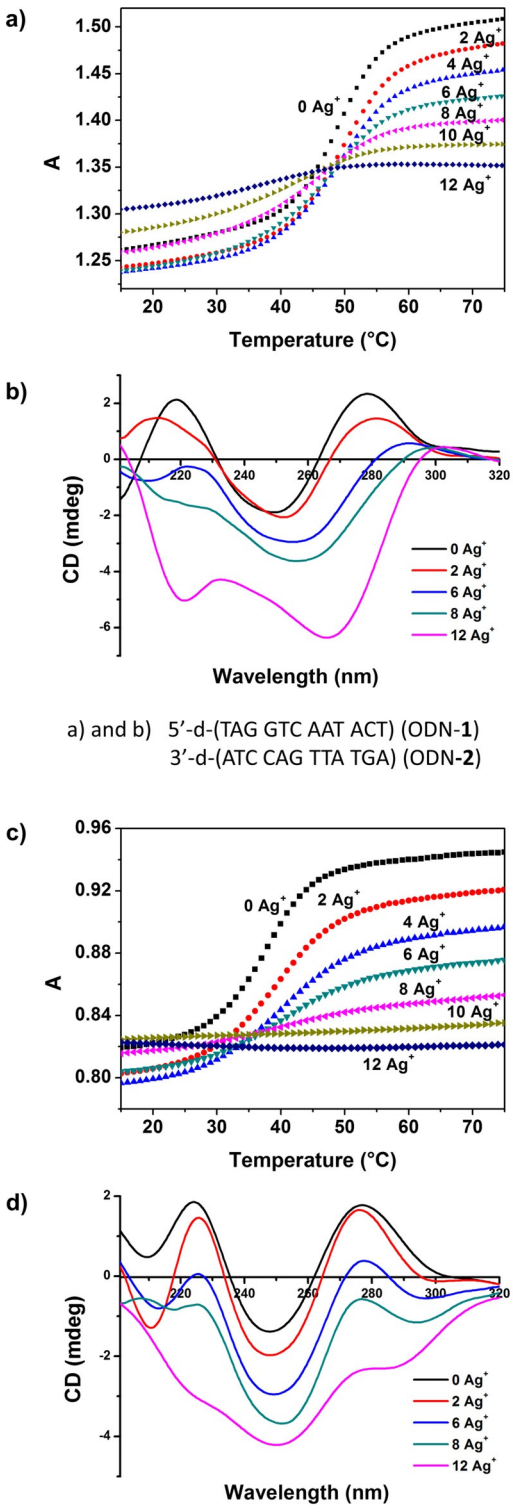

a) and b) 5′-d-(TAG GTC AAT ACT) (ODN-**1**)
3′-d-(ATC CAG TTA TGA) (ODN-**2**)

c) and d) 5′-d-(T^{7}A^{7}G ^{7}G TC ^{7}A^{7}A T ^{7}AC T) (ODN-**15**)
3′-d-(^{7}AT C C^{7}A^{7}G T T^{7}A T^{7}G^{7}A) (ODN-**16**)

Figure 6. Thermal denaturation experiments performed at a concentration of 5 μM + 5 μM single strand in buffer solution (100 mM NaOAc, 10 mM $Mg(OAc)_2$, pH 7.4), monitoring at 260 nm in the presence of various concentrations of Ag^+ (0 to 12 silver ions): a) ODN-**1**·ODN-**2**; c) ODN-**15**·ODN-**16**. CD spectra of the modified oligodeoxyribonucleotides. The spectra were measured in 100 mM NaOAc, 10 mM $Mg(OAc)_2$ buffer (pH 7.4) in the absence of Ag^+ or with 2, 6, 8, or 12 Ag^+ ions at a concentration of 5 μM + 5 μM single strand: b) ODN-**1**·ODN-**2**; d) ODN-**15**·ODN-**16**.

favor of a silver-rich duplex that does not melt. Both species coexist, and the sigmoidal melting profile is caused exclusively by the original duplex. After the addition of 12 silver ions, the sigmoidal melting curve turned into an almost straight line with a very low absorbance change upon heating, and the absorbance was close to that of the initial silver-free duplex. At this point, the silver-free duplex was completely converted into a duplex with silver-mediated base pairs.

Next, CD spectra were measured to visualize changes in the helical structure of the DNA (Figure 6b, d). B-DNA, as well as the silver-free duplexes, show conventional CD spectra with a positive lobe around 275 nm and a negative band near 245 nm. Similar spectra are also observed for the unmodified canonical duplex ODN-**1**·ODN-**2** as well the 7-deazapurine duplex ODN-**15**·ODN-**16**, in which all purine bases are replaced by the 7-deazapurine nucleosides c^7G_d and c^7A_d.

Upon the addition of silver ions, the CD spectra were dramatically altered. After the addition of two silver ions to the "purine" duplex ODN-**1**·ODN-**2**, bathochromic shifts of the bands at 275 and 245 nm were observed. Addition of 12 silver ions caused major changes. The positive band (originally at around 275 nm) disappeared and was replaced by a negative band at around 270 nm. The positive band at around 220 nm was replaced by a negative band with a bathochromically shifted maximum. This indicated that the B-DNA structure of the original silver-free Watson–Crick duplex was not maintained, and a silver-ion-rich complex was formed. Similar observations have been made on a self-complementary 8-mer duplex that was crystallized in the presence of silver ions. This duplex formed an unusual structure containing silver-mediated G–G and C–C base pairs.[6b]

In the case of the 7-deazapurine duplex ODN-**15**·ODN-**16**, the results were rather different to those obtained for the purine duplex ODN-**1**·ODN-**2** (Figure 6c). T_m did not change significantly upon increasing the number of silver ions (Figures S5–S7, Supporting Information). The CD spectra displayed a smooth transition from the silver-free B-DNA duplex to the non-melting duplex with 12 silver ions. Although the ellipticity of the band near 280 nm changed from positive to negative, the wavelength maximum of the band did not change in the same way as observed for the "purine" duplex. We believe that the differences between purine and 7-deazapurine duplexes are mainly due to extremely stable silver-mediated Hoogsteen-type pairs of dG residues, in which silver ions can bridge nitrogen atoms at position-7.[6,8g] This interaction is not available in the case of 7-deaza-2′-deoxyguanosine residues. Here, only the pyrimidine sites of the 7-deazapurine bases can be used for silver-ion binding.

Next, the duplex ODN-**10**·ODN-**8**, with two separated heterochiral α/β-dC base pairs, was investigated. A strong initial change of the melting curve was observed when two silver ions were added, and T_m increased from 24 °C to 40 °C (Figure 7a). This stemmed mainly from the transition from single strands to a duplex induced by the establishment of silver-mediated base pairs. Two silver ions were bound to the mismatch sites, forming two silver-mediated base pairs. According to Figure 7c, the situation is similar to that in the homochiral

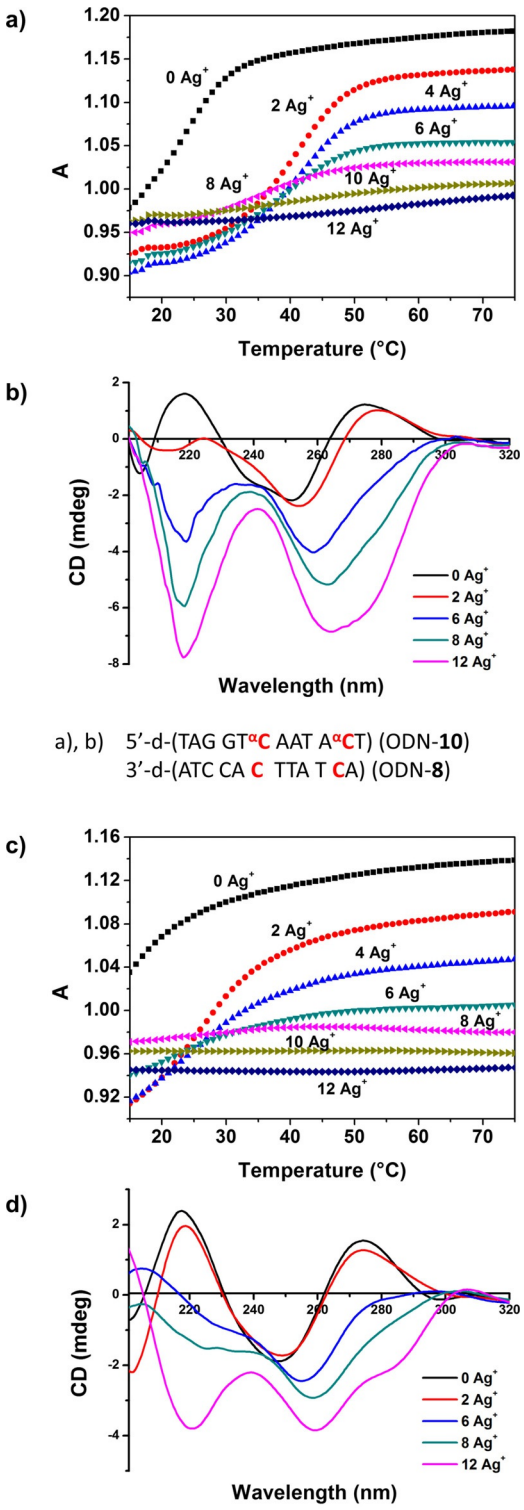

a), b) 5′-d-(TAG GT$^{\alpha}$**C** AAT A$^{\alpha}$**C**T) (ODN-**10**)
3′-d-(ATC CA **C** TTA T **C**A) (ODN-**8**)

c), d) 5′-d-(TAG GT**C** AAT A**C**T) (ODN-**1**)
3′-d-(ATC CA**C** TTA T **C**A) (ODN-**8**)

Figure 7. Thermal denaturation experiments performed at a concentration of 5 μM + 5 μM single strand in buffer solution (100 mM NaOAc, 10 mM $Mg(OAc)_2$, pH 7.4), monitoring at 260 nm in the presence of various concentrations of Ag^+ (0 to 12 silver ions): a) ODN-**10**·ODN-**8**; c) ODN-**1**·ODN-**8**. b,d) CD spectra of the modified oligodeoxyribonucleotides. The spectra were measured in 100 mM NaOAc, 10 mM $Mg(OAc)_2$ buffer (pH 7.4) in the absence of Ag^+ or with 2, 6, 8, or 12 Ag^+ ions/duplex at a concentration of 5 μM + 5 μM single strand: b) ODN-**10**·ODN-**8**; d) ODN-**1**·ODN-**8**.

duplex ODN-**1**·ODN-**8**. The only difference is its lower stability. Again, the addition of 12 silver ions resulted in a new silver-rich duplex that did not melt (Figures S5–S7, Supporting Information). CD spectra (Figure 7 b, d) were consistent with this behavior.

From the results of melting experiments of duplexes with homochiral and heterochiral mismatches in the absence and presence of silver ions, it is concluded that the silver-ion-free solution at 25 °C consisted of a mixture of single strands and duplexes (Figure 8). When silver ions were added, silver-mediated duplexes were formed and single strands were consumed.

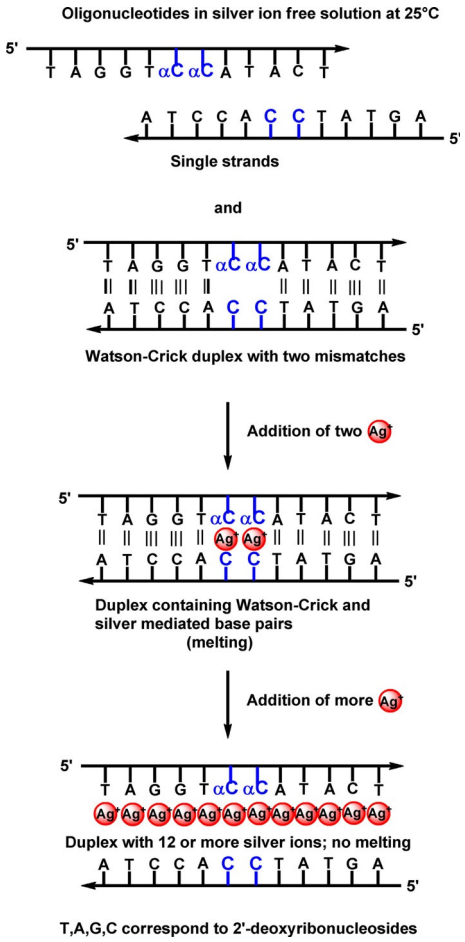

Figure 8. Schematic view of the different proposed single-strand and duplex species derived from the oligonucleotides ODN-**11** and ODN-**4** in solution at 25 °C.

As silver-mediated dC–dC base-pair formation was accompanied by the formation of regular dG–dC and dA–dT Watson–Crick base pairs, there was a strong initial decrease in UV absorbance. As the T_m of the homochiral duplex is lower than that of its heterochiral counterpart, solutions with homochiral oligonucleotides contain more single strands and the UV change is stronger.

Additional silver ions induced formation of the silver-rich duplex, which did not melt and coexisted with the duplex containing only two silver-mediated mismatches. Only the latter

duplex melted, and its concentration decreased as more silver ions were added. Ultimately, only the non-melting silver-rich duplex was present. Through argentophilic interactions, this species could aggregate to form silver wires. Such a silver wire has recently been reported by Ono[6a] for another 12-mer duplex incorporating two dC–dC mismatches. As the original melting curves with increasing amount of silver ions were not given, and only the normalized profiles were shown, we synthesized the related self-complementary oligonucleotide 5′-d(GGACTCGACTCC) (ODN-**17**), in which the mismatches were formed by two dC–dC pairs instead of one dC–dC pair and one ^{Br}dC–dC pair. The same experiments as discussed above were then performed in NaOAc buffer as used in our study as well as in 3-(*N*-morpholino)propanesulfonic acid (MOPS) buffer as used by Ono[6a] (Figures S14 and S15, Supporting Information). The duplex ODN-**17**·ODN-**17** and our 12-mer duplexes showed very similar behavior in melting and CD experiments[6a] when they were treated with a large number of silver ions. We therefore conclude that our silver-rich duplexes also form silver-mediated base pairs in solution, as described for the crystal of duplex ODN-**17**·ODN-**17**. The phenomenon of wire formation might also be possible, as promoted by argentophilic interactions between the duplexes. Overhanging ends may not be required. So-called "sticky ends", as used in enzymatic ligation, might be sufficient for wire formation.

The silver-rich duplex can contain silver-mediated dA–dT and dG–dC pairs and/or silver-mediated base pairs of dG–dG, dC–dC, and dT–dT. It should be noted that silver-mediated base pairing follows other stability rules than those for Watson–Crick pairs.[8g] According to published work on silver-mediated base-pair formation, silver-ion-mediated base pairing between canonical nucleobases is less specific than Watson–Crick base pairing. Nevertheless, in duplexes with homochiral or heterochiral cytosine base pairs, the B-DNA structure was maintained as long as the silver-ion concentration was low. At high silver-ion concentration, silver-rich complexes displaying different CD spectra were formed.

Conclusions

Silver-mediated base pairs have been constructed with consecutive and isolated heterochiral α-dC–dC mismatches incorporated in a 12-mer oligonucleotide duplex at various positions of the double-helix. For comparison, DNA duplexes with homochiral dC–dC base pairs placed at exactly the same positions as their heterochiral counterparts have also been prepared. To this end, a new synthesis of the α-D anomer of dC has been developed. The thermal stabilities of the duplexes have been evaluated by T_m measurements in the presence and absence of silver ions. Figure 9 displays the stability changes for homochiral and heterochiral duplexes with mismatches at exactly the same positions in the absence (blue bars) and presence of silver ions (red bars). It is obvious from the T_m data that the nearest neighbors of silver-mediated base pairs have an impact on silver-mediated duplex stability. Moreover, consecutive, as opposed to separated, incorporation of silver-mediated pairs leads to distinct stability changes. In all cases, silver-mediated heterochiral base pairs are more stable than homochiral dC–dC pairs. Duplexes with silver-mediated homochiral cytosine base pairs are always less stable than those with Watson–Crick pairs, whereas the stability of duplexes with silver-mediated heterochiral pairs approaches that of duplexes with canonical Watson–Crick pairs.

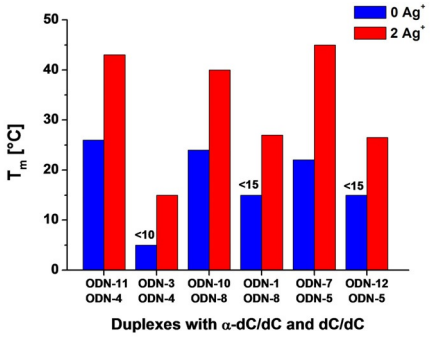

5'-d(TAGGT$^{\alpha}$C$^{\alpha}$CATACT) ODN-**11**
3'-d(ATCCA C C TATGA) ODN-**4**

5'-d(TAGGTCCATACT) ODN-**3**
3'-d(ATCCACCTATGA) ODN-**4**

5'-d(TAGGT$^{\alpha}$CAATA$^{\alpha}$CT) ODN-**10**
3'-d(ATCCA C TT AT CA) ODN-**8**

5'-d(TAGGTCAATACT) ODN-**1**
3'-d(ATCCACTT ATCA) ODN-**8**

5'-d(TA$^{\alpha}$CGT$^{\alpha}$CAATACT) ODN-**7**
3'-d(AT C CA C TT ATGA) ODN-**5**

5'-d(TACGTCAATACT) ODN-**12**
3'-d(ATCCAC TT ATGA) ODN-**5**

Figure 9. Top) Bar diagram showing T_m increases before (blue bars) and after addition of silver ions (red bars) for heterochiral α-dC/β-dC and homochiral β-dC/β-dC duplexes (for duplex sequences, see the bottom part).

When the number of silver ions was equal to the number of base pairs of the duplex (12), a non-melting silver-rich complex was formed. All duplexes studied in this work showed this behavior. At moderate silver-ion concentrations, silver-rich duplexes can coexist with silver-ion-poor duplexes. The new silver-rich complexes can contain silver-mediated dA–dT and dG–dC pairs and/or silver-mediated dG–dG, dC–dC, and dT–dT pairs, as reported for a similar duplex based on a solid-state X-ray investigation.[6a] The structural changes were supported by CD experiments, which showed that the B-DNA structure was maintained at low silver-ion concentration, whereas silver-rich duplexes showed completely different CD spectra. The unmodified duplex ODN-**1**·ODN-**2** without cytosine mismatches and its 7-deazapurine counterpart (ODN-**15**·ODN-**16**), in which all purine bases are replaced by c^7G_d and c^7A_d, showed different behavior because, in the latter case, silver ions cannot bridge the nitrogen atoms at position-7. Our experiments have indicated that silver-mediated base-pair formation between canonical nucleobases is a complex process and follows other stability rules than Watson–Crick base pairing.[8g] Nevertheless, in duplexes with homochiral or heterochiral cytosine pairs, the B-DNA structure is maintained as long as the silver-ion concentration is low. At high silver-ion concentration, silver-rich complexes displaying different CD spectra are formed.

Experimental Section

General methods and materials: All chemicals and solvents were of laboratory grade as obtained from commercial suppliers and

were used without further purification. Reversed-phase HPLC was carried out on a 4×250 mm RP-18 (10 μm) LiChrospher 100 column on a Hitachi 655 A-12 liquid chromatograph equipped with an L6200A intelligent pump and a 655 A variable-wavelength UV monitor. The molecular masses of the oligonucleotides were determined by MALDI-TOF mass spectrometry on a Bruker Autoflex Speed spectrometer operated in linear positive mode with 3-hydroxypicolinic acid (3-HPA) as the matrix. Thermal melting curves were measured with an Agilent Technologies Cary 100 Bio UV/Vis spectrophotometer equipped with a thermoelectric controller. The temperature in the reference cell was continuously monitored by means of a Pt-100 resistor, applying a heating rate of 1 °C min^{-1}. T_m values were determined from the melting curves using the software *Meltwin*, version 3.0.[19] CD spectra were recorded at 25 °C on a JASCO J-815 spectrometer. ^{13}C NMR data are shown in Table S1 (Supporting Information).

Oligonucleotide syntheses and characterization: Solid-phase oligonucleotide syntheses were performed on an ABI 392-08 synthesizer at 1 μmol scale (trityl-on mode) employing the phosphoramidite of α-dC (**10**) with standard building blocks, giving average coupling yields of over 95%. After cleavage from the solid support, the oligonucleotides were deprotected in 28% aqueous ammonia at 55 °C for 2 h. The DMT-containing oligonucleotides were purified by reversed-phase HPLC (RP-18) with a gradient system of (A) MeCN, (B) 0.1 M (Et_3NH)OAc (pH 7.0)/MeCN, 95:5; gradient I: 0–3 min 10–15% A in B, 3–15 min 15–50% A in B; flow rate 0.7 mL min^{-1}, monitoring at 260 nm. The purified "trityl-on" oligonucleotides were treated with 2.5% $CHCl_2COOH/CH_2Cl_2$ for 2 min at 0 °C to remove the DMT residues. The detritylated oligomers were again purified by reversed-phase HPLC with gradient II: 0–20 min 0–20% A in B; 20–25 min 20% A in B; flow rate 0.7 mL min^{-1}. The oligonucleotides were desalted on a reversed-phase column (RP-18) using water to elute the salt, and then the oligonucleotides were eluted with H_2O/MeOH (2:3). The oligonucleotides were lyophilized on a Speed-Vac evaporator to yield colorless solids, which were frozen at −24 °C. The purity of all oligonucleotides was confirmed by RP-18 HPLC (Figure S13, Supporting Information) and MALDI-TOF mass spectrometry (Table 1). The extinction coefficients ε_{260} (H_2O) of the nucleosides were determined as: dA 15400, dG 11700, dT 8800, dC 7300, and α-dC 7300 mol^{-1} dm^{-3} cm^{-1}. The extinction coefficients of the oligonucleotides were calculated from the sum of the extinction coefficients of their constituent nucleosides, with a hypochromic change of 20% for the single strands.

Anomeric mixture of 1-[2-deoxy-3,5-di-*O*-(*p*-toluoyl)-α-D-*erythro*-pentofuranosyl]cytosine (5) and 1-[2-deoxy-3,5-di-*O*-(*p*-toluoyl)-β-D-*erythro*-pentofuranosyl]cytosine (6): Cytosine **3** (4.0 g, 36 mmol) was suspended in 1,1,1,3,3,3-hexamethyldisilazane (HMDS, 36 mL). Trimethylsilyl chloride (510 μL, 9.5 mmol) was then added, and the reaction mixture was heated to reflux for 2 h, during which the solid dissolved. After cooling to RT, the excess HMDS was removed under reduced pressure and the solid brownish residue was dissolved in CH_2Cl_2 (40 mL). After addition of 4-nitrophenol (1.6 g, 11.5 mmol), pyridine (870 μL, 10.8 mmol), and 3,5-di-*O*-(*p*-toluoyl)-α-D-*erythro*-pentofuranosyl chloride (**4**) (12.7 g, 32.7 mmol), the reaction mixture was stirred for 24 h at RT. The solvent was then removed under reduced pressure and the anomeric mixture was purified by FC (silica gel column, 15×4 cm, CH_2Cl_2/MeOH, 9:1) to remove impurities. Evaporation of the volatiles from the main zone containing an inseparable mixture of anomers gave a colorless foam (13.2 g, 84%) in a ratio of 2:1 (α/β), as determined from the H-1′ signals in the ^{1}H NMR spectrum of the anomeric mixture. R_f = 0.5 (**5** and **6**) (CH_2Cl_2/MeOH, 9:1); ^{1}H NMR (600 MHz, [D$_6$]DMSO, 26 °C): δ = 8.44 (br s, 0.66 H; NH_a), 8.19 (br s, 0.33 H; NH_b), 7.99 (d, J = 7.2 Hz, 0.66 H; H-6$_a$), 7.90–7.92 (m, 2.64 H; arom. H), 7.85 (d, J = 8.4 Hz, 0.66 H; arom. H), 7.79 (d, J = 7.8 Hz, 0.33 H; H-6$_b$), 7.75–7.79 (m, 1.32 H; Ar-H), 7.35–7.37 (m, 1.32 H; Ar-H), 7.31 (d, J = 7.8 Hz, 0.66 H; Ar-H), 7.28–7.29 (m, 1.32 H; Ar-H), 6.26 (t, J = 6.6 Hz, 0.33 H; H-1′$_b$), 6.14 (dd, J = 6.3, 1.2 Hz, 0.66 H; H-1′$_a$), 5.91 (d, J = 7.8 Hz, 1 H; H-5$_a$), 5.85 (d, J = 7.8 Hz, 1 H; H-5$_b$), 5.56–5.58 (m, 0.33 H; H-3′$_b$), 5.52 (d, J = 6.0 Hz, 0.66 H; H-3′$_a$), 5.04 (t, J = 4.8 Hz, 0.66 H; H-4′$_a$), 4.56–4.58 (m, 0.66 H; H-5′$_a$), 4.51–4.53 (m, 0.33 H; H-4′$_b$), 4.56–4.67 (m, 1.32 H; H-5′$_a$, H-5′$_b$), 2.86–2.91 (m, 0.66 H; H-2′$_{\beta a}$), 2.56–2.60 (m, 0.33 H; H-2′$_{\beta b}$), 2.51–2.54 (m, 0.33 H; H-2′$_{\alpha b}$), 2.44 ppm (d, J = 9.0 Hz, 0.66 H, H-2′$_{\alpha a}$); ^{13}C NMR (150 MHz, [D$_6$]DMSO, 26 °C): δ = 165.47 (C=O$_b$), 165.44 (C=O$_a$), 165.21 (C=O$_b$), 164.96 (C=O$_a$), 163.45 (C-4$_b$), 162.79 (C-4$_a$), 152.16 (C-2$_b$), 151.13 (C-2$_a$), 142.86 (C-6$_a$), 142.02 (C-6$_b$), 94.40 (C-5$_b$), 93.07 (C-5$_a$), 87.99 (C-1′$_a$), 85.91 (C-1′$_b$), 84.33 (C-4′$_a$), 81.51 (C-4′$_b$), 74.73 (C-3′$_a$), 74.66 (C-3′$_b$), 64.24 (C-5′$_b$), 64.05 (C-5′$_a$), 37.93 (C-2′$_a$), 36.89 ppm (C-2′$_b$); HRMS (ESI-TOF): *m/z* calcd for $C_{25}H_{25}N_3O_6Na$: 486.1636 [*M*+Na]$^+$; found: 486.1636.

Anomeric mixture of 1-(2-deoxy-α-D-*erythro*-pentofuranosyl)cytosine (1, α-dC) and 1-(2-deoxy-β-D-*erythro*-pentofuranosyl)cytosine (2, β-dC): The anomeric mixture of **5** and **6** (4.0 g, 9.2 mmol) was suspended in 0.2 M NaOMe/MeOH (100 mL) and stirred for 1 h at RT. The solvent was evaporated and the remaining residue was adsorbed on silica gel and subjected to FC (silica gel column, 12×4 cm, CH_2Cl_2/MeOH, 8:2). An anomeric mixture of **1** and **2** (1.96 g, 94%) was obtained from the main zone as a colorless solid. R_f = 0.5 (CH_2Cl_2/MeOH, 8:2); ^{1}H NMR (600 MHz, [D$_6$]DMSO, 26 °C): δ = 7.79 (d, J = 7.2 Hz, 0.33 H; H-6$_b$), 7.75 (d, J = 7.2 Hz, 0.66 H; H-6$_a$), 7.24 (br s, 0.33 H; NH_b), 7.19 (br s, 0.66 H; NH_a), 7.08 (br s, 0.33 H; NH_b), 7.00 (br s, 0.66 H; NH_a), 6.14 (*t*, J = 7.2 Hz, 0.33 H; H-1′$_b$), 6.03 (dd, J = 7.2, 3.0 Hz, 0.66 H; H-1′$_a$), 5.74 (d, J = 7.8 Hz, 0.33 H; H-5$_b$), 5.72 (d, J = 7.2 Hz, 0.66 H; H-5$_a$), 5.24 (d, J = 3.6 Hz, 0.66 H; HO-3′$_a$), 5.23 (d, J = 4.2 Hz, 0.33 H; HO-3′$_b$), 5.02 (t, J = 5.4 Hz, 0.33 H; HO-5′$_b$), 4.86 (t, J = 6.0 Hz, 0.66 H; HO-5′$_a$), 4.18–4.19 (m, 1 H; H-3′$_a$, H-3′$_b$), 4.12–4.14 (m, 0.66 H; H-4′$_a$), 3.75–3.77 (m, 0.33 H; H-4′$_b$), 3.50–3.57 (m, 0.66 H; H-5′$_b$), 3.37–3.39 (m, 1.32 H; 2H-5′$_b$, H-5′$_a$), 2.47–2.52 (m, 0.66 H; H-2′$_{\beta a}$), 2.08–2.11 (m, 0.33 H; H-2′$_{\alpha b}$), 1.90–1.94 (m, 0.33 H; H-2′$_{\alpha b}$), 1.81 ppm (dd, J = 2.4, 14.4 Hz; H-2′$_{\alpha a}$); ^{13}C NMR (150 MHz, [D$_6$]DMSO, 26 °C): δ = 165.58 (C-4$_a$), 165.48 (C-4$_b$), 155.17 (C-2$_a$), 155.07 (C-2$_a$), 141.67 (C-6$_b$), 140.97 (C-6$_a$), 93.96 (C-5$_b$), 93.17 (C-5$_a$), 89.09 (C-4′$_a$), 87.19 (C-4′$_b$), 86.42 (C-1′$_a$), 84.84 (C-1′$_b$), 70.59 (C-3′$_a$), 70.39 (C-3′$_b$), 61.75 (C-5′$_a$), 61.33 (C-5′$_b$), 40.59 (C-2′$_a$), 40.34 ppm (C-2′$_b$); HRMS (ESI-TOF): *m/z* calcd for $C_9H_{13}N_3O_4Na$: 250.0798 [*M*+Na]$^+$; found: 250.0807.

Benzoylation of the anomeric mixture of 1 and 2: The anomeric mixture of **1** and **2** (2.0 g, 8.8 mmol) was dissolved in anhydrous DMF (10 mL). Benzoic anhydride (3.0 g, 13.3 mmol) was added and the reaction mixture was stirred for 48 h at RT. The solvent was then evaporated and the remaining residue was adsorbed on silica gel and subjected to FC (silica gel column, 20×4 cm, CH_2Cl_2/MeOH, 100:0→92:8).

***N*^{4}-Benzoyl-1-(2-deoxy-α-D-*erythro*-pentofuranosyl)cytosine (7)**:[21] From the slower migrating main zone, compound **7** was obtained as a colorless foam (1.04 g, 36%). R_f = 0.5 (CH_2Cl_2/MeOH, 9:1); ^{1}H NMR (600 MHz, [D$_6$]DMSO, 26 °C): δ = 11.06 (br s, 1 H; NH), 8.21 (d, J = 7.2 Hz, 1 H; H-6), 8.00–8.01 (m, 2 H; Ar-H), 7.61–7.63 (m, 1 H; Ar-H), 7.51–7.52 (m, 2 H; Ar-H), 7.34 (d, J = 7.2 Hz, 1 H; H-5), 6.04 (dd, J = 5.7, 5.6 Hz, 1 H; H-1′), 5.13 (d, J = 2.4 Hz, 1 H; HO-3′), 4.90 (t, J = 5.4 Hz, 1 H; HO-5′), 4.32–4.33 (m, 1 H; H-4′), 4.23–4.24 (m, 1 H; H-3′), 3.40–3.47 (m, 2 H; H-5′), 2.54–2.58 (m, 1 H; H-2′$_\beta$), 2.00–2.02 ppm (m, 1 H; H-2′$_\alpha$); ^{13}C NMR (150 MHz, [D$_6$]DMSO, 26 °C): δ = 167.19 (C=O), 162.93 (C-4), 154.50 (C-2), 145.68 (C-6), 133.24 (Ar-C), 132.64 (Ar-C), 129.24 (Ar-C), 128.42 (Ar-C), 95.26 (C-5), 90.32 (C-4′),

88.22 (C-1′), 70.60 (C-3′), 61.71 (C-5′), 40.65 ppm (C-2′); HRMS (ESI-TOF): *m/z* calcd for $C_{16}H_{17}N_3O_5Na$: 354.1060 $[M+Na]^+$; found: 354.1070.

N^4-Benzoyl-1-(2-deoxy-β-D-*erythro*-pentofuranosyl)cytosine (8): From the faster migrating main zone, compound **8** was obtained as a colorless foam (640 mg, 22%). $R_f = 0.6$ (CH_2Cl_2/MeOH, 9:1); ^{1}H NMR (600 MHz, [D$_6$]DMSO, 26 °C): $\delta = 11.23$ (brs, 1H; NH), 8.39 (d, $J = 7.5$ Hz, 1H; H-6), 7.99–8.01 (m, 2H; Ar-H), 7.61–7.63 (m, 1H; Ar-H), 7.50–7.52 (m, 2H; Ar-H), 7.34 (d, $J = 7.2$ Hz, 1H; H-5), 6.14 (t, $J = 6.0$ Hz, 1H; H-1′), 5.13 (s, 1H; HO-3′), 5.08 (s, 1H; HO-5′), 4.24 (m, 1H; H-3′), 3.88 (m, 1H; H-4′), 3.58–3.65 (m, 2H; 2×H-5′), 2.30–2.33 (m, 1H; H-2′$_\beta$), 2.04–2.08 ppm (m, 1H; H-2′$_\alpha$); ^{13}C NMR (150 MHz, [D$_6$]DMSO, 26 °C): $\delta = 167.50$ (C=O), 162.95 (C-4), 154.37 (C-2), 144.96 (C-6), 133.20 (Ar-C), 132.72 (Ar-C), 129.17 (Ar-C), 128.45 (Ar-C), 95.06 (C-5), 87.94 (C-4′), 86.21 (C-1′), 69.92 (C-3′), 60.94 (C-5′), 40.91 ppm (C-2′); HRMS (ESI-TOF): *m/z* calcd for $C_{16}H_{17}N_3O_5Na$: 354.1060 $[M+Na]^+$; found: 354.1074.

N^4-Benzoyl-1-[2-deoxy-5-*O*-(4,4′-dimethoxytrityl)-α-D-*erythro*-pentofuranosyl]cytosine (9): Compound **7** (170 mg, 0.51 mmol) was dissolved in pyridine (3 mL) and 4,4′-dimethoxytrityl chloride (226 mg, 0.67 mmol) was added. The reaction mixture was stirred for 3 h at RT. The resulting solution was then diluted with CH_2Cl_2 (20 mL), washed with 5% aq. $NaHCO_3$ (20 mL), and dried over Na_2SO_4. After removal of the solvent, the oily residue was subjected to FC (silica gel column, 12×4 cm, CH_2Cl_2/MeOH, 8:2). From the main zone, compound **9** was obtained as a colorless foam (292 mg, 90%). $R_f = 0.3$ (CH_2Cl_2/MeOH, 8:2); ^{1}H NMR (600 MHz, [D$_6$]DMSO, 26 °C): $\delta = 11.18$ (s, 1H; NH), 8.25 (d, $J = 7.79$ Hz, 1H; H-6), 7.99–8.02 (m, 2H; Ar-H), 7.62–7.64 (m, 1H; Ar-H), 7.48–7.54 (m, 2H; Ar-H), 7.21–7.41 (m, 10H; Ar-H), 6.90–6.93 (m, 4H; Ar-H), 6.14 (d, $J = 5.7$ Hz, 1H; H-1′), 5.22 (d, $J = 2.7$ Hz, 1H; HO-3′), 4.47–4.49 (m, 1H; H-4′), 4.20–4.22 (m, 1H; H-3′), 3.75 (s, 6H; OCH_3), 3.12–3.14 (m, 1H; H-5′), 3.01–3.03 (m, 1H; H-5′), 2.57–2.66 (m, 1H; H-2′$_\beta$), 2.04–2.08 ppm (m, 1H; H-2′$_\alpha$); ^{13}C NMR (150 MHz, [D$_6$]DMSO, 26 °C): $\delta = 167.2$ (C=O), 163.01 (C-4), 158.1 (Ar-C), 154.5 (C-2), 145.7 (C-6), 144.8 (Ar-C), 135.4 (Ar-C), 135.3 (Ar-C), 133.2 (Ar-C), 132.7 (Ar-C), 129.7 (Ar-C), 128.9 (Ar-C), 128.4 (Ar-C), 127.9 (Ar-C), 127.7 (Ar-C), 126.7 (Ar-C), 113.2 (Ar-C), 95.3 (C-5), 88.5 (C-4′), 88.3 (C-1′), 70.97 (C-3′), 63.9 (C-5′), 55.0 (OCH_3), 40.7 ppm (C-2′); HRMS (ESI-TOF): *m/z* calcd for $C_{37}H_{35}N_3O_7Na$: 656.2367 $[M+Na]^+$; found: 656.2358.

N^4-Benzoyl-1-[2-deoxy-5-*O*-(4,4′-dimethoxytrityl)-α-D-*erythro*-pentofuranosyl]cytosine 3′-(2-cyanoethyl)-*N*,*N*-diisopropylphosphoramidite (10): (iPr)$_2$NEt (120 μL, 0.7 mmol) and 2-cyanoethyl diisopropylphosphoramidochloridite (130 μL, 0.615 mmol) were added to a solution of **9** (260 mg, 0.41 mmol) in dry CH_2Cl_2 (20 mL). The reaction mixture was stirred for 30 min at RT. After complete conversion, as monitored by TLC, the solution was diluted with CH_2Cl_2 (24 mL) and poured into $NaHCO_3$ solution (5%, 30 mL). The aqueous phase was extracted with CH_2Cl_2 (10 mL) and the combined organic layers were dried (Na_2SO_4). After removal of the solvent, the oily residue was subjected to FC (silica gel column, 12×3 cm, CH_2Cl_2/acetone, 95:5). Evaporation of the solvents from the main zone afforded **10** (274 mg, 81%) as a yellowish foam. R_f = 0.4 and 0.6 (CH_2Cl_2/acetone, 80:20); ^{31}P NMR (121 MHz, $CDCl_3$, 20 °C): $\delta = 149.24$, 148.37 ppm; HRMS (ESI-TOF): *m/z* calcd for $C_{46}H_{52}N_5O_8PNa$: 856.3446 $[M+Na]^+$; found: 856.3445.

1-(2-Deoxy-α-D-*erythro*-pentofuranosyl)cytosine (1): A suspension of **7** (500 mg, 1.4 mmol) in saturated NH_3/MeOH was transferred to a steel bomb and heated at 100 °C for 16 h. The solvent was then evaporated and the remaining residue was adsorbed on silica gel and subjected to FC (silica gel column, 12×4 cm, CH_2Cl_2/MeOH, 8:2). From the main zone, compound **1** (284 mg, 81%) was obtained as a colorless solid. $R_f = 0.2$ and 0.6 (CH_2Cl_2/MeOH, 80:20); ^{1}H NMR (600 MHz, [D$_6$]DMSO, 26 °C): $\delta = 7.74$ (d, $J = 7.4$ Hz, 1H; H-6), 7.07 (brs, 1H; NH), 6.99 (brs, 1H; NH), 6.04 (dd, $J = 6.0$, 7.4 Hz, 1H; H-1′), 5.69 (d, $J = 7.2$ Hz, 1H; H-5), 5.18 (d, $J = 3.2$ Hz, 1H; HO-3′), 5.08 (t, $J = 5.7$ Hz, 1H; HO-5′), 4.17–4.19 (m, 1H; H-3′), 4.11–4.13 (m, 1H; H-4′), 3.37–3.39 (m, 2H; H-5′), 2.47–2.52 (m, 1H; H-2′$_\beta$), 1.81 ppm (dt, $J = 14.1$, 2.6 Hz, 1H; H-2′$_\alpha$); ^{13}C NMR (150 MHz, [D$_6$]DMSO, 26 °C): $\delta = 165.67$ (C-4), 155.23 (C-2), 141.62 (C-6), 93.10 (C-5), 89.09 (C-4′), 86.43 (C-1′), 70.61 (C-3′), 61.77 (C-5′), 40.62 ppm (C-2′); HRMS (ESI-TOF): *m/z* calcd for $C_9H_{13}N_3O_4Na$: 250.0798 $[M+Na]^+$; found: 250.0801.

Acknowledgements

We thank Dr. Simone Budow-Busse for critical reading of the manuscript. We would like to thank Dr. M. Letzel, Universität Münster, Germany, for acquiring the ESI MALDI-TOF spectra, and Prof. Dr. B. Wünsch, Institut für Pharmazeutische und Medizinische Chemie, Universität Münster, Germany, for providing us with 600 MHz NMR spectra. We also thank Prof. Dr. T. J. Schmidt, Institut für Pharmazeutische Biologie und Phytochemie, Universität Münster, Germany, for facilitating the measurement of CD spectra.

Conflict of interest

The authors declare no conflict of interest.

Keywords: base pairing · circular dichroism · DNA · nucleobases · silver

[1] a) A. Ono, H. Torigoe, Y. Tanaka, I. Okamoto, *Chem. Soc. Rev.* **2011**, *40*, 5855–5866; b) M. H. Shamsi, H.-B. Kraatz, *J. Inorg. Organomet. Polym.* **2013**, *23*, 4–23; c) P. Scharf, J. Müller, *ChemPlusChem* **2013**, *78*, 20–34; d) Y. Takezawa, J. Müller, M. Shionoya, *Chem. Lett.* **2017**, *46*, 622–633; e) Y. Takezawa, M. Shionoya, *Acc. Chem. Res.* **2012**, *45*, 2066–2076; f) G. H. Clever, C. Kaul, T. Carell, *Angew. Chem. Int. Ed.* **2007**, *46*, 6226–6236; *Angew. Chem.* **2007**, *119*, 6340–6350; g) D.-L. Ma, H.-Z. He, D. S.-H. Chan, C.-H. Leung, *Chem. Sci.* **2013**, *4*, 3366–3380; h) Y. Tanaka, J. Kondo, V. Sychrovský, J. Šebera, T. Dairaku, H. Saneyoshi, H. Urata, H. Torigoe, A. Ono, *Chem. Commun.* **2015**, *51*, 17343–17360.

[2] a) T. Yamane, N. Davidson, *Biochim. Biophys. Acta* **1962**, *55*, 609–621; b) M. Daune, C. A. Dekker, H. K. Schachman, *Biopolymers* **1966**, *4*, 51–76; c) R. M. Izatt, J. J. Christensen, J. H. Rytting, *Chem. Rev.* **1971**, *71*, 439–481; d) G. L. Eichhorn, J. J. Butzow, P. Clark, E. Tarien, *Biopolymers* **1967**, *5*, 283–296; e) R. H. Jensen, N. Davidson, *Biopolymers* **1966**, *4*, 17–32; f) V. A. Bloomfield, D. M. Crothers, I. Tinoco, Jr., in *Physical Chemistry of Nucleic Acids* (Ed.: L. Wernick), Harper & Row, Publishers, Inc., New York, **1974**, pp. 420–429.

[3] a) H. Torigoe, A. Ono, A. Takamori, *Nucleic Acids Symp. Ser.* **2004**, *48*, 101–102; b) A. Ono, S. Cao, H. Togashi, M. Tashiro, T. Fujimoto, T. Machinami, S. Oda, Y. Miyake, I. Okamoto, Y. Tanaka, *Chem. Commun.* **2008**, 4825–4827.

[4] J. Kondo, Y. Tada, T. Dairaku, H. Saneyoshi, I. Okamoto, Y. Tanaka, A. Ono, *Angew. Chem. Int. Ed.* **2015**, *54*, 13323–13326; *Angew. Chem.* **2015**, *127*, 13521–13524.

[5] a) S. K. Jana, X. Guo, H. Mei, F. Seela, *Chem. Commun.* **2015**, *51*, 17301–17304; b) H. Mei, S. A. Ingale, F. Seela, *Chem. Eur. J.* **2014**, *20*, 16248–16257; c) H. Yang, H. Mei, F. Seela, *Chem. Eur. J.* **2015**, *21*, 10207–10219; d) H. Mei, I. Röhl, F. Seela, *J. Org. Chem.* **2013**, *78*, 9457–9463.

[6] a) J. Kondo, Y. Tada, T. Dairaku, Y. Hattori, H. Saneyoshi, A. Ono, Y. Tanaka, *Nat. Chem.* **2017**, *9*, 956–960; b) H. Liu, F. Shen, P. Haruehanroengra, Q. Yao, Y. Cheng, Y. Chen, C. Yang, J. Zhang, B. Wu, Q. Luo, R.

Cui, J. Li, J. Ma, J. Sheng, J. Gan, *Angew. Chem. Int. Ed.* **2017**, *56*, 9430 – 9434; *Angew. Chem.* **2017**, *129*, 9558 – 9562.

[7] a) N. Santamaría-Díaz, J. M. Méndez-Arriaga, J. M. Salas, M. A. Galindo, *Angew. Chem. Int. Ed.* **2016**, *55*, 6170 – 6174; *Angew. Chem.* **2016**, *128*, 6278 – 6282; b) J. M. Méndez-Arriaga, C. R. Maldonado, J. A. Dobado, M. A. Galindo, *Chem. Eur. J.* **2018**, *24*, 4583 – 4589.

[8] a) N. Zimmermann, E. Meggers, P. G. Schultz, *J. Am. Chem. Soc.* **2002**, *124*, 13684 – 13685; b) B. Lippert, P. J. Sanz Miguel, *Acc. Chem. Res.* **2016**, *49*, 1537 – 1545; c) S. Naskar, R. Guha, J. Müller, *Angew. Chem.* **2019**, *131*, 58; d) H. Zhao, P. Leonard, X. Guo, H. Yang, F. Seela, *Chem. Eur. J.* **2017**, *23*, 5529 – 5540; e) X. Guo, P. Leonard, S. A. Ingale, F. Seela, *Chem. Eur. J.* **2017**, *23*, 17740 – 17754; f) S. Taherpour, O. Golubev, T. Lönnberg, *J. Org. Chem.* **2014**, *79*, 8990 – 8999; g) S. M. Swasey, L. E. Leal, O. Lopez-Acevedo, J. Pavlovich, E. G. Gwinn, *Sci. Rep.* **2015**, *5*, 10163 – 10171; h) H. Urata, E. Yamaguchi, Y. Nakamura, S.-i. Wada, *Chem. Commun.* **2011**, *47*, 941 – 943; i) D. A. Megger, C. F. Guerra, F. M. Bickelhaupt, J. Müller, *J. Inorg. Biochem.* **2011**, *105*, 1398 – 1404; j) X. Zhou, D. Kondhare, P. Leonard, F. Seela, *Chem. Eur. J.* **2019**, *25*, 10408 – 10419.

[9] X. Guo, F. Seela, *Chem. Eur. J.* **2017**, *23*, 11776 – 11779.

[10] S. L. Müller, X. Zhou, P. Leonard, O. Korzhenko, C. Daniliuc, F. Seela, *Chem. Eur. J.* **2019**, *25*, 3077 – 3090.

[11] M. Hoffer, *Chem. Ber.* **1960**, *93*, 2777 – 2781.

[12] J. J. Fox, N. C. Yung, I. Wempen, M. Hoffer, *J. Am. Chem. Soc.* **1961**, *83*, 4066 – 4070.

[13] a) A. Holý, *Collect. Czech. Chem. Commun.* **1973**, *38*, 100 – 114; b) H. Sawai, A. Nakamura, H. Hayashi, K. Shinozuka, *Nucleosides Nucleotides* **1994**, *13*, 1647 – 1654; c) D. H. Shannahoff, R. A. Sanchez, *J. Org. Chem.* **1973**, *38*, 593 – 598.

[14] T. Yamaguchi, M. Saneyoshi, *Chem. Pharm. Bull.* **1984**, *32*, 1441 – 1450.

[15] a) K. Shinozuka, N. Yamada, A. Nakamura, H. Ozaki, H. Sawai, *Bioorg. Med. Chem. Lett.* **1996**, *6*, 1843 – 1848; b) Z. Wang, D. R. Prudhomme, J. R. Buck, M. Park, C. J. Rizzo, *J. Org. Chem.* **2000**, *65*, 5969 – 5985; c) F. Morvan, J. Zeidler, B. Rayner, *Tetrahedron* **1998**, *54*, 71 – 82; d) M. Prystaš, J. Farkaš, F. Šorm, *Collect. Czech. Chem. Commun.* **1965**, *30*, 3123 – 3133; e) R. Kurfürst, V. Roig, M. Chassignol, U. Asseline, N. T. Thuong, *Tetrahedron* **1993**, *49*, 6975 – 6990.

[16] H. Aoyama, *Bull. Chem. Soc. Jpn.* **1987**, *60*, 2073 – 2077.

[17] D. I. Ward, P. L. Coe, R. T. Walker, *Collect. Czech. Chem. Commun.* **1993**, *58*, 1 – 4.

[18] F. Morvan, B. Rayner, J.-P. Leonetti, J.-L. Imbach, *Nucleic Acids Res.* **1988**, *16*, 833 – 847.

[19] J. A. McDowell, D. H. Turner, *Biochemistry* **1996**, *35*, 14077 – 14089.

[20] X. Guo, P. Leonard, S. A. Ingale, J. Liu, H. Mei, M. Sieg, F. Seela, *Chem. Eur. J.* **2018**, *24*, 8883 – 8892.

[21] F. Morvan, B. Rayner, J.-L. Imbach, D.-K. Chang, J. W. Lown, *Nucleic Acids Res.* **1986**, *14*, 5019 – 5035.

Manuscript received: August 27, 2019
Revised manuscript received: October 2, 2019
Accepted manuscript online: October 4, 2019
Version of record online: November 28, 2019

